IVYSPRING INTERNATIONAL PUBLISHER

Theranostics

2016; 6(5): 726-738. doi: 10.7150/thno.14514

Research Paper

Thrombus-Targeted Theranostic Microbubbles: A New Technology towards Concurrent Rapid Ultrasound Diagnosis and Bleeding-free Fibrinolytic Treatment of Thrombosis

Xiaowei Wang[1,2]✉*, Yannik Gkanatsas[1,3]✉*, Jathushan Palasubramaniam[1], Jan David Hohmann[1], Yung Chih Chen[1], Bock Lim[1], Christoph E Hagemeyer[1,4], Karlheinz Peter[1,2,4]

1. Baker IDI Heart & Diabetes Institute, Melbourne, Australia.
2. Department of Medicine, Monash University, Melbourne, Australia.
3. Department of Experimental Pharmacology and Toxicology, University Medical Center Hamburg-Eppendorf, Hamburg, Germany;
4. Department of Immunology, Monash University, Melbourne, Australia.

*Equally contributing first authors.

✉ Corresponding authors: Dr Xiaowei Wang; Prof Karlheinz Peter, Atherothrombosis & Vascular Biology, Baker IDI Heart and Diabetes Institute, 75 Commercial Road, Melbourne VIC 3004 Australia. Fax: +61(0)385321100, Tel: +61(0)385321495 Email: xiaowei.wang@bakeridi.edu.au; karlheinz.peter@bakeridi.edu.au.

Received: 2015.11.24; Accepted: 2016.02.08; Published: 2016.03.20

Abstract

Rationale: Myocardial infarction and stroke are leading causes of morbidity/mortality. The typical underlying pathology is the formation of thrombi/emboli and subsequent vessel occlusion. Systemically administered fibrinolytic drugs are the most effective pharmacological therapy. However, bleeding complications are relatively common and this risk as such limits their broader use. Furthermore, a rapid non-invasive imaging technology is not available. Thereby, many thrombotic events are missed or only diagnosed when ischemic damage has already occurred.

Objective: Design and preclinical testing of a novel 'theranostic' technology for the rapid non-invasive diagnosis and effective, bleeding-free treatment of thrombosis.

Methods and Results: A newly created, innovative theranostic microbubble combines a recombinant fibrinolytic drug, an echo-enhancing microbubble and a recombinant thrombus-targeting device in form of an activated-platelet-specific single-chain antibody. After initial *in vitro* proof of functionality, we tested this theranostic microbubble both in ultrasound imaging and thrombolytic therapy using a mouse model of ferric-chloride-induced thrombosis in the carotid artery. We demonstrate the reliable highly sensitive detection of *in vivo* thrombi and the ability to monitor their size changes in real time. Furthermore, these theranostic microbubbles proofed to be as effective in thrombolysis as commercial urokinase but without the prolongation of bleeding time as seen with urokinase.

Conclusions: We describe a novel theranostic technology enabling simultaneous diagnosis and treatment of thrombosis, as well as monitoring of success or failure of thrombolysis. This technology holds promise for major progress in rapid diagnosis and bleeding-free thrombolysis thereby potentially preventing the often devastating consequences of thrombotic disease in many patients.

Key words: platelets, theranostics, thrombolysis, glycoprotein IIb/IIIa, microbubbles.

Introduction

Cardiovascular diseases such as myocardial infarction (MI) and stroke are leading causes of death worldwide. The typical underlying pathology is the formation of thrombi and vessel occlusion either at the origin of thrombosis or at sites of embolization. One key contributor to thrombosis, especially in the case of MI, is atherosclerosis, which is driven by an inflammatory response caused by mechanisms such as oxidation and accumulation of lipids in the artery wall[1,2]. This results in adhesion of activated platelets and monocytes at the site of vascular inflammation[1,2].

Although chronic atherosclerotic lesions can significantly obstruct the vessel lumen and thus reduce blood flow, most acute cases of MI and many cases of stroke are caused by plaque rupture triggering the exposure of thrombogenic material and inducing the activation of the coagulation cascade, platelet activation/aggregation, and subsequent vessel blockage[3,4]. Many other cases of stroke are caused by embolization of thrombotic material that originates from ruptured atherosclerotic lesions or heart chambers in the setting of atrial fibrillation. This ultimately leads to vessel occlusion, a medical emergency, which requires timely diagnosis and immediate action to reperfuse the affected vessels and salvage the ischemic tissue.

There is clearly a significant medical need for the rapid diagnosis of acute thrombosis as, for example, in the case of coronary thrombosis leading to MI. So far there is no non-invasive imaging technology available that allows the detection of coronary thrombi. Our current work provides a unique approach for diagnosis and targeted therapy based on molecular ultrasound imaging. Among all imaging modalities, ultrasound has several advantages that prompted us to use it for the development of a unique theranostic approach. It is non-invasive, carries no radiation-associated risk, has no side-effects, and is inherently real time. Ultrasound scanners are highly portable and are already available in most hospitals. Therefore molecular ultrasound imaging could provide a safe, rapid, and cost-effective technique for detection of thrombosis[5].

Platelets play a pivotal role in thrombosis, and the most abundant receptor expressed on the platelet surface is the glycoprotein (GP) IIb/IIIa complex, also known as integrin αIIbβ3 (CD41/CD61), which is the main fibrinogen/fibrin receptor-mediating platelet aggregation[6,7]. When platelets are activated, GPIIb/IIIa undergoes a conformational change from a low-affinity to a high-affinity state, allowing the binding of fibrinogen, which leads to platelet aggregation and thrombus formation[6,7]. These features make GPIIb/IIIa an ideal target for both molecular imaging of thrombosis and delivery of thrombolytic drugs. We have developed conformation-specific anti–GPIIb/IIIa single-chain antibodies (scFvs), which bind specifically to a ligand-induced binding site (LIBS) on activated GPIIb/IIIa[6–8], and thereby constitute a unique targeting tool for molecular imaging and targeted therapy of thrombosis.

We have previously demonstrated the ability of $scFv_{anti\text{-}LIBS}$ to detect activated platelets in MRI[9–12] and PET[13] for thrombosis and inflammation. We have also developed a non-invasive molecular ultrasound imaging method for the diagnosis of thrombosis[14] via the conjugation of $scFv_{anti\text{-}LIBS}$ onto ultrasound-enhancing microbubbles (MBs). These targeted MBs bind to activated GPIIb/IIIa receptors on activated platelets, thereby allowing real-time imaging of thrombosis, as well as monitoring of success or failure of pharmacological thrombolysis[14]. The advantages of such a rapid and accurate diagnosis would be greatly enhanced if non-invasive targeted thrombolysis could be performed concurrently using activated-platelet–targeted and drug-loaded MBs.

Non-invasive thrombolytic reperfusion use of plasminogen activators (PAs), such as streptokinase, tissue plasminogen activators (tPA), and urokinase plasminogen activators (uPAs), is available in current clinical settings. While these drugs are beneficial[15], side-effects such as bleeding complications and neurotoxicity (in the case of tPA) have been described, thereby hampering their wide clinical use[16]. Past and ongoing substantial research efforts have focused on identifying new strategies to eliminate such complications. We have recently developed a promising approach using single-chain antibodies to deliver drugs to evolving or established blood clots, enabling enhanced and localized therapy with no or reduced risk of bleeding[17,18]. We have demonstrated that our recombinant single-chain urokinase plasminogen activators (scuPA) result in efficient thrombolysis[18].

Here we present a non-invasive theranostic (simultaneously diagnostic and therapeutic) approach for the diagnosis of thrombi, as well as fibrinolytic treatment and monitoring of success or failure of thrombolysis. By dual conjugation of both $scFv_{anti\text{-}LIBS}$ and scuPA to form targeted theranostic microbubbles (TT-MBs), we demonstrate that these TT-MBs are well suited for diagnosis in molecular ultrasound imaging and for thrombolytic therapy of thrombi *in vivo* in the carotid artery of mice. These theranostic MBs allow the detection of reduced thrombus size triggered by their therapeutic payload. Overall, the presented

targeted molecular imaging approach has strong potential to be translated to clinical application in humans.

Methods

A detailed description of the methods is provided in the online-only Supplementary material.

Single-chain antibodies and single-chain urokinase plasminogen activator

The $scFv_{anti\text{-}LIBS}$ construct was generated, expressed, and purified as previously described[14]. Briefly, the recombinant scuPA with an LPETG peptide motif at the C-terminus was cloned into the pSecTag2A vector system for expression in human embryonic kidney cells (HEK293F). The purity of the recombinant proteins was analyzed using SDS-PAGE and Western blotting. The addition of the LPETG motif allowed coupling of a GGG-biotin peptide to the scuPA construct using the recombinantly produced *S. aureus* transpeptidase sortase A[19,20].

Flow cytometry

Platelet-rich plasma (PRP) was obtained from healthy volunteers. Binding of $scFv_{anti\text{-}LIBS}$ constructs, to either non-activated or activated platelets, was assessed by an AlexaFluor 488-coupled anti-His-tag antibody using a FACS Calibur (BD Bioscience, USA).

Enzymatic activity assays

Urokinase activity was determined with the S2444 and the conversion of plasminogen to plasmin with the S2251 chromogenic substrate (both Chromogenix, Italy). Comparison between clinically used uPA (Medac GmbH, Germany) and scuPA was made on the basis of equal urokinase activity.

Flow-chamber adhesion assay

Whole blood was perfused through glass capillaries, which were coated overnight with 100µg/ml collagen. $scFv_{anti\text{-}LIBS}$ and scuPA were added to target-ready microbubbles (VisualSonics Inc., Canada), to form targeted theranostic microbubbles (TT-MBs).

In vivo ultrasound molecular imaging in mice

All experiments involving animals were approved by the Alfred Medical Research and Education Precinct Animal Ethics Committee (E/1406/2013/B). Ultrasound of mice was performed with a Vevo2100 high-resolution imaging system (VisualSonics Inc., Canada). Thrombi were induced in the left carotid artery with a 6% ferric-chloride injury.

Assessment of tail bleeding time

The mouse tail was transected 5mm from the tip and submersed in saline at 37˚C. Bleeding time was determined as the time needed for the cessation of a visible blood flow for at least 1 min.

Statistical analysis

Data is expressed as mean ± standard error of the mean (SEM), unless otherwise specified. Flow cytometry and thrombolysis data were analyzed with two-way ANOVA repeated measures analysis using Bonferroni's multiple-comparison post-test.

Results

Cloning, purification, and biotinylation of scuPA constructs

The generation of a scuPA construct suitable for bioconjugation to microbubbles was achieved by the addition of an LPETG tag at the C-terminus of scuPA (Figure 1A). This five amino acid tag serves as a recognition sequence for the recombinantly produced S. aureus transpeptidase Sortase, which catalyzes a peptide bond formation with GGG-Biotin to scuPA-LPETGGG-Biotin[19,20]. The success of DNA amplification, purification, and restriction digest of scuPA fragments was evaluated by agar gel electrophoresis. The construct was visualized in comparison to a marker after amplification with PCR and restriction digest (Figure 1B). The pSectag2A plasmid was visualized at ~ 5kB after restriction digest. After the scuPA construct was cloned into the pSectag2A plasmid, transformed, and purified, gel electrophoresis was performed. The sequence of the scuPA construct was confirmed via DNA sequencing. After production of scuPA, Western blotting was used to demonstrate successful purification (Figure 1C). Western blotting was also used to demonstrate successful biotinylation of the scuPA construct (Figure 1C).

Cloning, purification, and biotinylation of $scFv_{anti\text{-}LIBS}$

The $scFv_{anti\text{-}LIBS}$ construct was cloned into a vector to incorporate a C-terminal AviTag™, a tag that encodes the protein avidin, which enables the scFv to bind to biotin (Figure 1D). The success of DNA amplification, purification, and restriction digest was evaluated by agarose gel electrophoresis (Figure 1E). After production of scFv, Western blotting was used to demonstrate successful purification and *in vivo* biotinylation of the recombinant protein (Figure 1F).

Proof of function of scuPA constructs

Urokinase activity was monitored by incubating scuPA with urokinase substrate S2444L (Figure 2A) in comparison with commercial uPA. The scuPA construct and standards using commercial uPA at

different concentrations resulted in linear enzymatic activity over 40 min. Conversion of plasminogen to plasmin was monitored using the S2251 amidolytic assay (Figure 2B). The activity of plasmin generation of 10nmol/L of scuPA-biotin was compared against standards using commercial uPA (0U-2000U/ml). The standards were plotted on a graph and fitted with a linear regression, from which we obtained the equation to calculate and convert the activity of scuPA-biotin (Figure 2C).

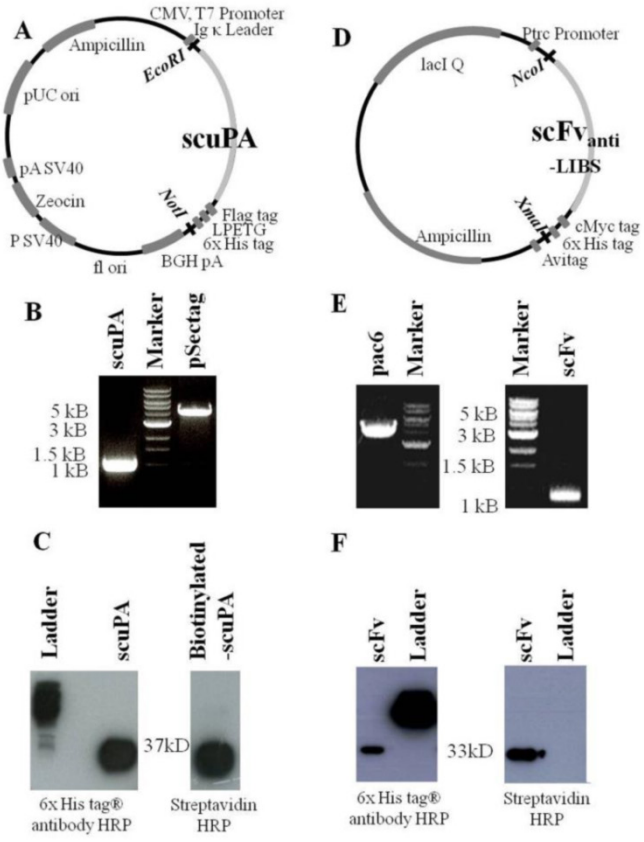

Figure 1: Vector-map, generation and purification of scuPA and scFv$_{anti-LIBS}$ for microbubble conjugation. A. Gene-map of scuPA in pSectag2A vector for mammalian expression. The restriction enzymes used to insert the construct are EcoRI and NotI. **B.** Electrophoresis with 0.8% agarose gel: pSectag2A plasmid (5137bp) after double cut restriction digest, and scuPA (924bp) after polymerase chain reaction amplification. **C.** Western blot analysis of scuPA after protein purification detected with an HRP-coupled anti-6x His-tag antibody, and proof of successful biotinylation of scuPA via Sortase A enzyme as detected using streptavidin HRP. **D.** Gene-map of scFv$_{anti-LIBS}$ in pAC6 vector for biotinylation. The restriction enzymes used to insert the construct are NcoI and XmaI. **B.** Electrophoresis with 0.8% agarose gel: pAC6 plasmid (4186bp) after double cut restriction digest, and scuPA (925bp) after polymerase chain reaction amplification. **C.** Western blot analysis of scFv$_{anti-LIBS}$ after protein purification detected with an HRP-coupled anti-6x His-tag antibody and proof of biotin on the scFv$_{anti-LIBS}$ as detected using streptavidin HRP.

In vitro proof of fibrinolytic potential of scuPA-biotin

Fibrinolysis in a 96-well plate assay was performed to determine the ability of the recombinant biotinylated scuPA to break down clots. Clot formation and clot breakdown were measured over 60 min (% of clot remaining). At 30 min, commercial uPA at 200U/ml and 400U/ml showed strong fibrinolysis of clots as compared to the vehicle control (Figure 3A; 4.839 ± 2.42 vs. 4.289 ± 1.7 vs. 88.32 ± 2.76, respectively; % clot remaining ± SEM; n=5; p<0.001). At 30 min, biotinlyated scuPA at 10nmol/L, 20nmol/L, and 40nmol/L also showed strong fibrinolysis as compared to the vehicle control (Figure 3A; 25 ± 11.92 vs. 13.03 ± 5.89 vs. 6.125 ± 1.34; n=5; p<0.001). Similar results were obtained at 45 min (Figure 3B & 3C; n=5).

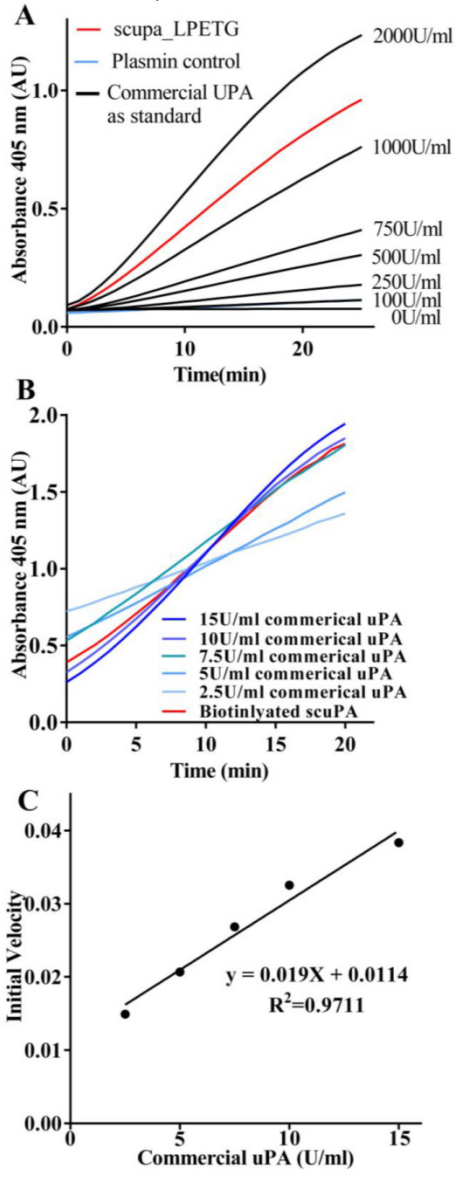

Figure 2: Proof of function of scuPA constructs. A. Urokinase activity assay of scuPA on 96-well plates using urokinase substrate S2444L. Increase of absorption at 405nm was measured over a 40 min period. ScuPA and standards using commercial uPA at different concentrations resulted in linear enzymatic activity. **B.** Plasminogen conversion assay of scuPA on 96-well plates using S2251 amidolytic assay. The conversion of plasminogen to plasmin was monitored with the S2251 amidolytic assay. Generation of plasmin for scuPA at 10nmol/L was compared against standards of commercial uPA at different concentration. Increase of absorption at 405nm was measured over a 40 min period. **C.** Activity of scuPA was calculated from the initial velocities obtained from lines fitted to data of time versus plasmin generated for the standards at a range of 0 to 15U/ml commercial uPA.

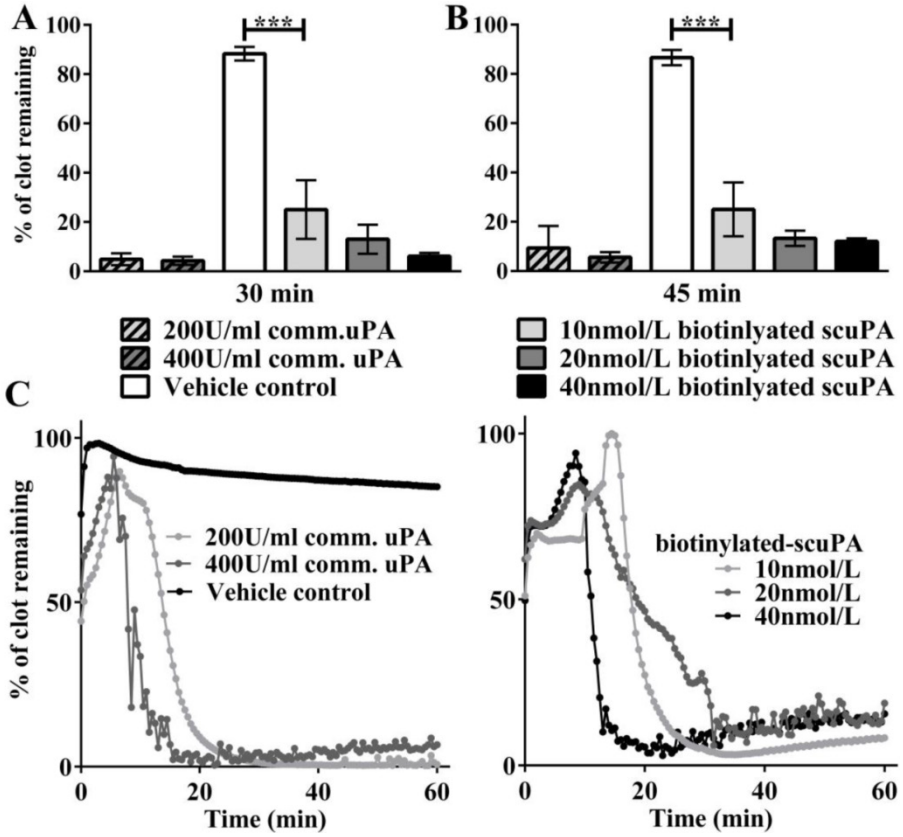

Figure 3: Fibrinolysis assay in a 96-well plate demonstrating successful thrombolysis with biotinylated scuPA. A. Bar chart showing % of clot remaining after 30 min of fibrinolysis. Commercial uPA at 200U/ml and 400U/ml showed strong fibrinolysis of clots as opposed to vehicle control, which did not show any fibrinolysis (n=5: p<0.001). Biotinlyated-scuPA at 10nmol/L, 20nmol/L and 40nmol/L also showed strong fibrinolysis as compared to the vehicle control (n=5; ***p<0.001). **B.** Bar chart showing % of clot remaining after 45 min of fibrinolysis. Similar results were obtained. **C.** Representative traces of the fibrinolysis assays are shown.

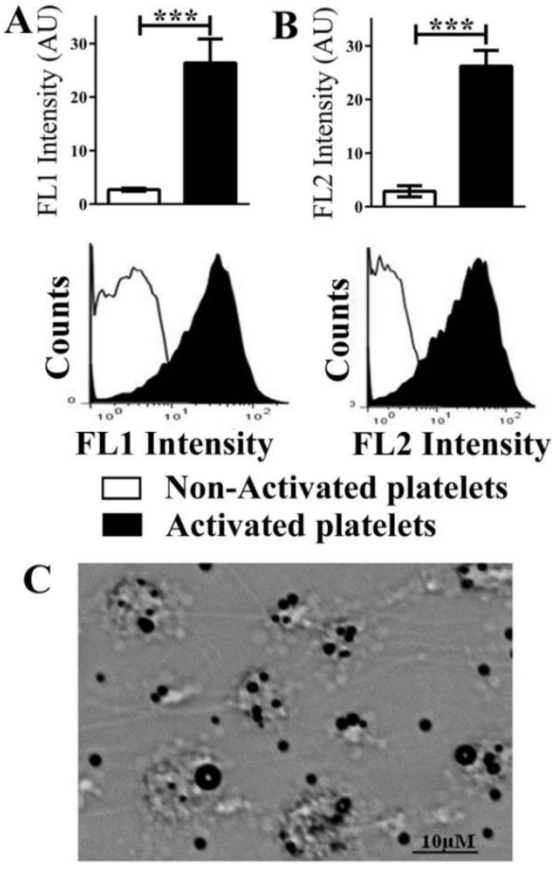

Figure 4: Flow cytometry demonstrating the functionality of scFv$_{anti-LIBS}$ and efficiency of *in vivo* biotinylation. A. Functionality of scFv$_{anti-LIBS}$ was proven with an AlexaFluor 488-coupled anti-Penta-His antibody in flow cytometry. Bar graphs depict the median fluorescence intensity values of five independent experiments. Representative fluorescence histograms are shown underneath the bar graphs. **B.** Functionality of scFv$_{anti-LIBS}$ as well as the efficiency of *in vivo* biotinylation was evaluated using R-phycoerythrin streptavidin in flow cytometry (mean ± SD, ***p<0.001). These assays were analyzed using a paired t-test. **C.** Representative microscopy images of targeted-theranostic microbubbles (TT-MBs) attached to activated platelets on microthrombi in a flow chamber experiment.

In vitro binding of scFv$_{anti-LIBS}$ constructs as assessed by flow cytometry

After the production of scFv$_{anti-LIBS}$, its binding capacity in relation to ADP-activated platelets was evaluated with an AlexaFluor 488-coupled anti-Penta-His antibody and R-phycoerythrin streptavidin in flow cytometry (Figure 4A & 4B). Incubation of ADP-activated platelets with scFv$_{anti-LIBS}$ resulted in an increase in fluorescence intensity as compared to non-activated platelets (26.36 ± 4.46 vs 2.69 ± 0.29 AU; n=5; p<0.001) using an AlexaFluor 488-coupled anti-Penta-His antibody. Similar results were obtained when the efficiency of *in vivo* biotinylation and scFv functionality was determined using R-phycoerythrin streptavidin in flow cytometry (26.2 ± 2.95 vs 2.87 ± 1.05 AU; n=5; p<0.001). Dual

fluorescence staining for platelets using an anti-CD62P monoclonal antibody, and $scFv_{anti\text{-}LIBS}$ using an AlexaFluor 488-coupled anti-Penta-His monoclonal antibody were performed to demonstrate the specific binding of $scFv_{anti\text{-}LIBS}$ to activated platelets (Additional File 1: Supplemental Figure 1). In addition, dual fluorescence staining for platelets using PAC-1, and $scFv_{anti\text{-}LIBS}$ using R-phycoerythrin streptavidin was performed to demonstrate the specific binding of $scFv_{anti\text{-}LIBS}$ to activated GPIIb/IIIa receptors on activated platelets (Additional File 1: Supplemental Figure 1).

In vitro proof of attachment of targeted theranostic microbubbles to microthrombi

Flow-chamber adhesion assays were used to demonstrate the attachment of TT-MBs to microthrombi after the conjugation of $scFv_{anti\text{-}LIBS}$ and scuPA to microbubbles (Figure 4C).

In vivo proof of theranostic molecular ultrasound imaging and simultaneous lysis of thrombi

Molecular ultrasound imaging was used to monitor thrombus size, particularly reduction in size. Ultrasound imaging of the mouse carotid artery on ultrasound typically shows luminal blood as black or dark grey, and microbubbles appear as a bright white color in the vessel lumen. Thrombi were visualized as white and bright signals after injection with platelet-targeted ultrasound contrast (LIBS-MB) on real-time ultrasound imaging. The baseline area, obtained 5 min after injection, was set to 100%. Imaging was preformed every 5 min for 45 min and the thrombus area was calculated. Mice were injected with either LIBS-MB and a vehicle control using saline (n=3), TT-MB (n=4), LIBS-MB, and a high dose of commercial uPA (n=3), or LIBS-MB and a low dose of commercial uPA (n=4) (Figure 5).

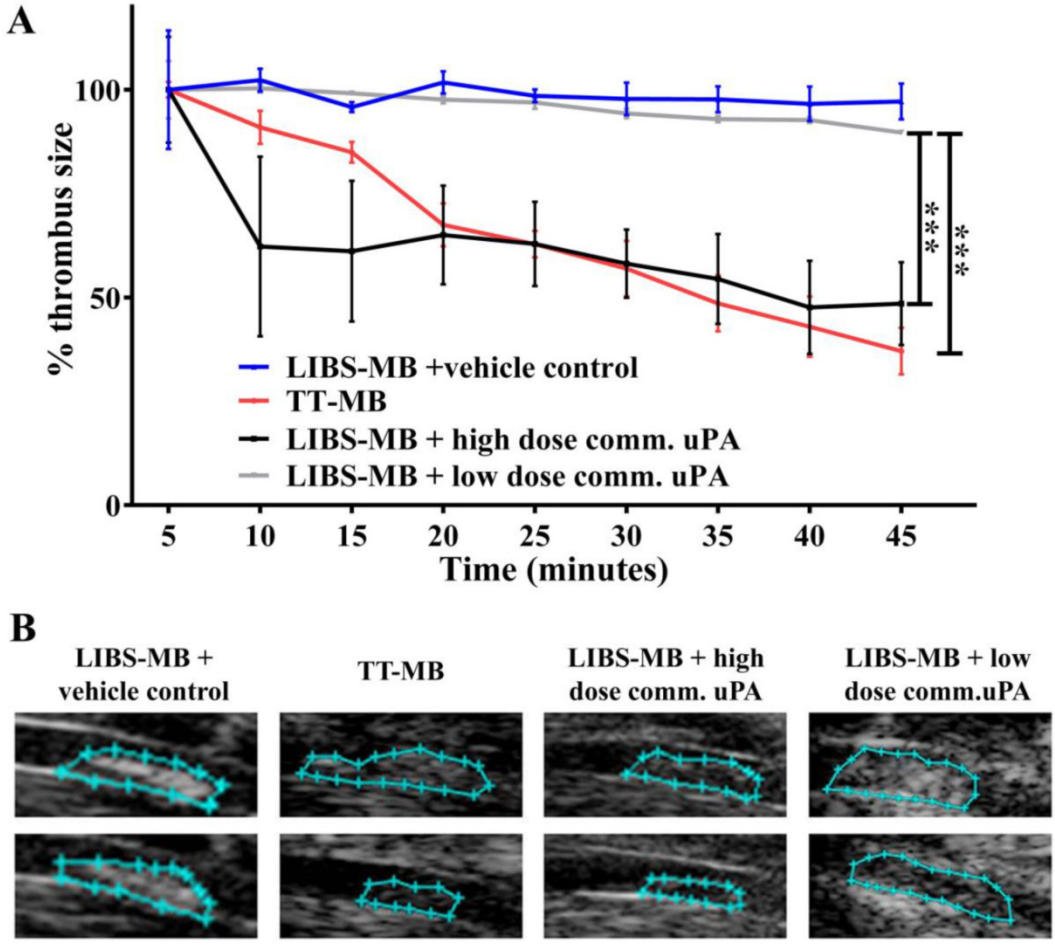

Figure 5: Monitoring of thrombolysis via molecular ultrasound imaging showed a theranostic effect and a reduction of thrombus size after the injection of TT-MB. A. A reduction of thrombus size was observed for animals administered with LIBS-MB and high dose of commercial uPA at 500U/g BW (black line and B) as compared to LIBS-MB and saline (blue line and C) as vehicle control. A reduction of thrombus size was also observed with TT-MB (red line and D) as compared to LIBS-MB and low dose of commercial uPA at 75U/g BW (light grey line and E). Baseline area was set to 100% and areas were calculated every 5 min for 45 min. Thrombus size was traced and calculated using VisualSonics software. Treatment groups were compared by use of repeated measures ANOVA over time with Bonferroni post tests at each time point (Mean % ± SEM; **p<0.01, ***p<0.001, n≥3 each).

Treatment with the TT-MBs significantly reduced thrombus size over the period 45 min, while no significant difference was observed in the LIBS-MB with saline vehicle control group (37.09 ± 5.6 vs. 97.16 ± 4.3; mean % ± SEM; $p<0.001$; $n>3$) (Figure 5; Videos 1–4 in Additional file 2 - Additional file 5). Thrombolysis was observed via ultrasound imaging using LIBS-MB and a high dose of commercial uPA. The ability of TT-MBs to target and dissolve thrombi was compared to that of mice injected with LIBS-MB and a high dose of commercial uPA, but there were no significant differences over the period of 45 min (37.09 ± 5.6 vs. 48.53 ± 9.9; ns; $n\geq3$).

The thrombolytic ability of TT-MBs was also compared with the LIBS-MB and a low dose of commercial uPA treatment group over 45 min. TT-MBs caused a reduction in thrombus size at 45 min post-administration compared to LIBS-MB and a low dose of commercial uPA (37.09 ± 5.6 vs. 89.72 ± 0.4; $p<0.001$; $n\geq3$). This LIBS-MB and low dose of commercial uPA treatment group was also compared against the LIBS-MB with saline vehicle control group. Administration of LIBS-MB and a low dose of commercial uPA showed no significant reduction in thrombus area compared to the saline group (89.72 ± 0.4 vs. 97.16 ± 4.3; ns; $n\geq3$).

The comparison of the thrombus area measured at the start of the treatment and at the end of the treatment showed a significant decrease in thrombus size for animals injected with TT-MB ($p<0.001$), as well as animals injected with LIBS-MB and treated with high dose of commercial uPA (positive control; $p<0.001$; Additional File 1: Supplemental Figure 2). No reduction in thrombus size was noted for animals injected with LIBS-MB and saline as negative controls or those treated with low dose of commercial uPA (NS)."

In additional to reduction in thrombus size, there was also a significant decrease in contrast intensity of the thrombus on molecular ultrasound imaging after treatment with TT-MB (Figure 6). The baselines of thrombus size and contrast intensity were set to 100% at the beginning of imaging. There was a significant reduction in the ultrasound contrast intensity for animals injected with TT-MB when compared to those injected with vehicle control (47.22 ± 4.2 vs. 82.25 ± 2.3; $p<0.01$; $n\geq3$). TT-MB treatment was as effective as a high dose of commercial uPA. The result in reduction of ultrasound contrast intensity is consistent with the data obtained in measuring reduction of thrombus size.

Histology of the carotid arteries from the four groups confirmed the sonographically observed differences in thrombus size (Figure 7).

Areas brighter than the reference image are presented in green after analysis with digital subtraction (ideos 1–4 in Additional file 2 - Additional file 5). Although thrombus identification and quantification using these B-mode images provide the necessary scientific and clinical information, digital subtraction and color highlighting were used for demonstration purposes and as an additional aid to facilitate immediate recognition of thrombi. Frames obtained before microbubble injection were subtracted from those obtained 45 min post-injection.

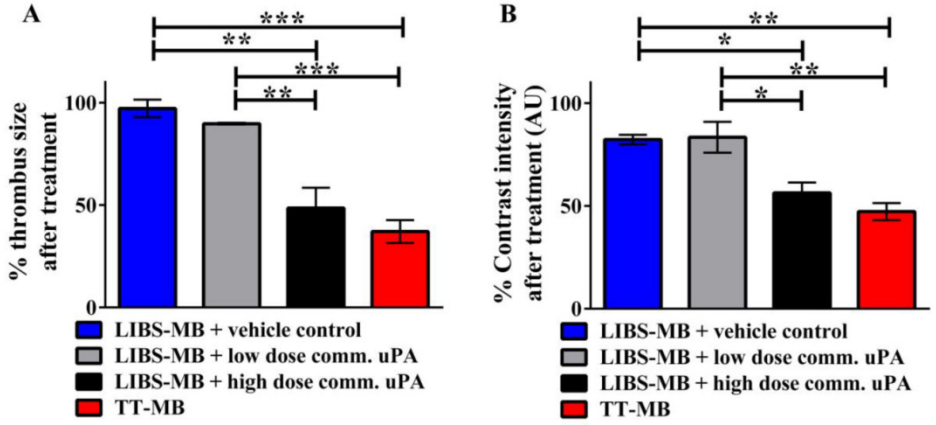

Figure 6: Quantitative measurement on molecular ultrasound imaging showing the reduction in both thrombus size and contrast intensity after treatment with TT-MB. A. Bar chart showing % of thrombus size at the end point of molecular ultrasound imaging. A reduction of thrombus size was observed for animals administered with LIBS-MB and high dose of commercial uPA at 500U/g BW (black) as compared to LIBS-MB and saline (blue) as vehicle control. The same significant reduction of thrombus size was also observed with TT-MB (red), but not with LIBS-MB and low dose of commercial uPA at 75U/g BW (light grey). B. Bar chart showing % contrast intensity at the end point of molecular ultrasound imaging. Results were similar to those of % thrombus size. Baseline area and contrast intensity was set to 100% and areas were measured at the start and end of imaging. Groups were compared by use of one-way ANOVA with Bonferroni post tests for multiple comparison (Mean % ± SEM, (*$p<0.05$, **$p<0.01$, ***$p<0.001$, $n\geq3$ each).

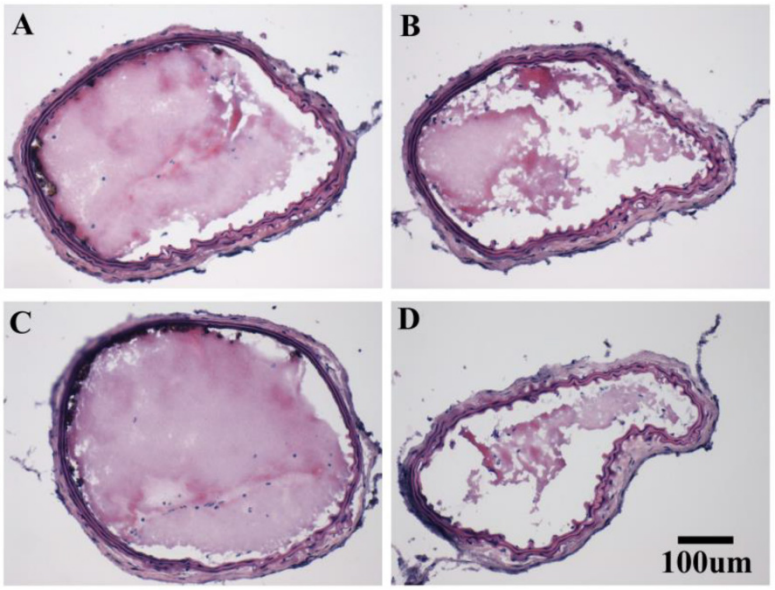

Figure 7: Representative images of hematoxylin and eosin stained thrombi in the carotid arteries of mice obtained after ultrasound imaging: A. after LIBS-MB and low dose commercial uPA, B. after TT-MB administration with a partially lysed thrombus, C. after LIBS-MB with saline as vehicle control and, D. after high dose commercial uPA with a partially lysed thrombus.

Effective targeted theranostic microbubbles do not cause bleeding time

Bleeding times were evaluated by surgical tail transection (Figure 8). LIBS-MB with a high dose of commercial uPA considerably prolonged bleeding compared to LIBS-MB with the saline vehicle control ($p<0.001$; n=4). In contrast, LIBS-MB with a low dose of commercial uPA and TT-MBs minimized bleeding time (ns; n=4). There was no difference between the bleeding times of animals given LIBS-MB with the vehicle control compared to TT-MBs (ns; n=4). Thus TT-MB has an anti-thrombotic effect without prolonging bleeding time.

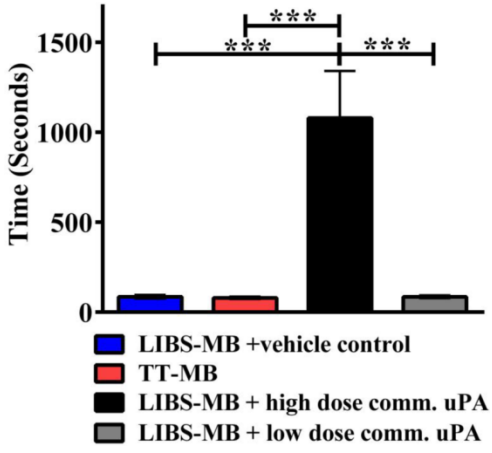

Figure 8: Bleeding time in mice determined by tail transection shows that there is no bleeding time prolongation at the effective dose of TT-MB. LIBS-MB with commercial uPA at 500U/g BW demonstrated considerably longer bleeding time as compared to LIBS-MB with saline vehicle control (*$p<0.001$, n=4 each). TT-MB, LIBS-MB with low dose commercial uPA at 75U/g BW and saline control did not prolong bleeding time. These assays were analyzed with one-way repeated measures ANOVA with the Bonferroni post test.

Discussion

Theranostic approaches combining diagnostic and therapeutic capabilities in a single agent/imaging microbubble have attracted major attention, as they promise specific, individualized therapies with fewer side-effects for various diseases. The main benefit of theranostic approaches is the ability to provide simultaneous diagnosis and treatment, as well as the ability to reliably and conveniently monitor the treatment outcome. Particularly for thrombotic diseases, an ultrasound theranostic approach could be broadly used in various clinical settings and promises to provide major benefits for a large number of patients.

Aiming for such a translationally highly attractive approach, we conjugated recombinant scFvs, which are specific for the activated GPIIb/IIIa receptor on platelets, and scuPA, a clinically approved fibrinolytic drug, to microbubbles, which thereby became a thrombus-specific imaging tool and a drug-carrying vehicle in one. To the best of our knowledge, this is the first demonstration of a theranostic approach to thrombotic disease using molecular ultrasound imaging based on MBs, which are dually conjugated both with scFvs in order to visualize thrombosis, as well as with scuPA in order to lyse thrombi.

Our data demonstrates that these targeted theranostic microbubbles can selectively bind to thrombi, thereby allowing successful molecular ultrasound imaging of thrombosis. The binding of the TT-MBs at the site of the clot allows enrichment of the thrombolytic drug in order to break down the fibrin

network without systemic adverse effects such as prolongation of bleeding time. This data describes the unique concept of a non-invasive, inexpensive, and widely available technology simultaneously detecting thrombi, resolving vessel occlusion, and monitoring success or failure of thrombolysis.

We have used recombinant scFvs, a minimal form of a functional antibody, as targeting tools since scFvs exhibit several major advantages: 1) scFvs lack the Fc region, are small in size, and are therefore minimally immunogenic; 2) they can be easily modified using molecular biology techniques to add specific tags for detection and/or bioconjugation; 3) their cost of production is relatively low[21]. In addition, the use of phage display in the generation of single-chain antibodies allows the selection of function-specific antibodies[22]. Such a unique scFv, specific for the activated conformation of GPIIb/IIIa, was used for the targeting of our theranostic microbubbles[14].

Ultrasound technology is an imaging modality that has evolved from a simple two-dimensional imaging tool used to assess crude anatomy to the current advanced three-dimensional, sensitive, high-resolution and sophisticated imaging platform. Employment of ultrasound contrast agents, such as microbubbles, provides the basis for molecular ultrasound imaging, which now exhibits a platform for functional characterization of diseased tissue without the necessity for surgical procedures or invasive biopsies[23,24]. Following advances in scanner technology, particularly in relation to resolving of contrasts, the development of targeted molecular ultrasound contrast agents has been driven by several pioneering groups, also covering the diagnosis of atherosclerosis[23,25–27]. In addition to its diagnostic use, ultrasound has been employed for therapeutic purposes. Given the rapidly improving technology of ultrasound scanners and the here-described development of contrast agents, theranostic ultrasound imaging offers an inexpensive, radiation-free, real-time, and portable alternative to MRI and nuclear imaging. With a growing ageing population and the consequent impact on healthcare costs, this new technology could be instrumental in allowing rapid and inexpensive diagnoses of MI and/or stroke, which would provide major benefits for a large number of patients.

There is no doubt that pharmacological thrombolysis can provide major benefits[15]. However, it comes with side-effects such as neurotoxicity and potentially fatal hemorrhagic complications[16]. In particular, the combination of anti-platelets and fibrinolytic agents shows a minimal improvement in mortality, safety, and efficacy, but results in increased bleeding complications[28]. Furthermore, many patients with MI or stroke are not given beneficial thrombolytic therapy because of their increased bleeding risk. Therefore, safety concerns have prompted research into more effective treatment in order to overcome the limitations associated with current pharmacological thrombolysis. As a consequence, there is a major need for novel reperfusion strategies; these include sonothrombolysis[29–36] and targeted-drug delivery[17,18,37–40].

The clinical use of microbubbles for echocardiography has been approved by the FDA in the United States, and for both echocardiography and radiology indications in Europe and Canada[41]. Pioneering groups demonstrated that the mechanical response of microbubbles to ultrasound can promote extravazation, and, even without the use of thrombolytic agents, has proven to be an effective thrombolytic approach both *in vitro* and *in vivo*[31,32,42]. Although these studies are mainly in the preclinical stage, they provide a strong basis for translation to clinical trials and offer a promising outlook for application in various cardiovascular diseases[33,35]. Culp *et al*.[31] demonstrated that infarct size decreases after treatment with sonothrombolysis using non-targeted MBs and Birnbaum *et al*.[43] observed recanalization of clots in the iliofemoral artery without significant side effects. Several clinical trials, such as the Combined Lysis of Thrombus in Brain Ischemia Using Transcranial Ultrasound and Systemic tPA (CLOTBUST)[44] and Transcranial Ultrasound in Clinical Sonothrombolysis (TUCSON)[45], examined the combination of non-targeted microbubbles, thrombolytic agents and ultrasound. These studies reported favorable results, such as improvement of recanalization rates and preservation of brain function. However, Molina *et al* [45] in the TUCSON trial also reported an increased number of intracranial hemorrhages.

Other research groups further improved the combination of MB application and fibrinolytic drugs using elegant targeting strategies[34,36,46,47]. Sonothrombolysis using targeted MBs allows the detection and localization of the thrombus. These studies looked into the feasibility of targeting the same integrin GPIIb/IIIa, using the arginine-glycine-aspartic acid (RGD) analog[34,46,47], and the non–activation-specific antibody fragment abciximab[36]. However, the RGD analogs are ligand mimetics that bind to all circulating platelets (both resting and activated), but also bind to other cells on the basis of their cross-reactivity toward other RGD-ligand–recognizing integrins.

Xie *et al*.[34] observed that using diagnostic

ultrasound and MRX-802 (RDG-MBs) in combination with a half-dose of recombinant pro-urokinase, heparin, and aspirin for 30 min improved epicardial recanalization rates and microvascular recovery. In another excellent study, Alonso *et al*.[36] reported that the use of abciximab immunobubbles and continuous diagnostic ultrasound over 30 min induced thrombolysis in rats. Since abciximab is a clinically used drug for preventing/treating platelet aggregation and thrombus formation, such an approach seems easily translatable. However, like RGD, abciximab binds to all circulating platelets and has been shown to cross-react with other integrin receptors[48]. An additional issue is that the binding of abciximab to non-activated GPIIb/IIIa receptors on circulating platelets results in an extended functional half life, and platelet inhibition over several days, thereby potentially increasing the risk of bleeding complications for a prolonged period[49].

Hua *et al*.[46] detailed in a recent publication that tPA-loaded RGD-MBs improved recanalization rates. These tPA-loaded RGD-MBs were given as a bolus followed by 30 min infusion, and ultrasound was performed on the site of interest over the time of infusion. The above studies infused the targeted or non-targeted microbubbles and thrombolytic agents, and sonoporated at various intensities or frequencies over time to obtain the desired thrombolysis or recanalization rate. However, safety concerns for patients in regard to the application of high-intensity, low-frequency ultrasound with microbubbles persist and have to be addressed in future studies.

Targeted drug delivery is another promising approach as a non-invasive pharmacological reperfusion strategy. In addition to platelet[6,17,18] and fibrin targeting[40], other epitopes, such as platelet endothelial cell adhesion molecule 1 (PECAM-1)[39] and glycophorin A on erythrocytes[38] have been targeted. Although thrombolysis has been demonstrated for both PECAM-1 and erythrocyte-targeting, these targets are not exclusive for thrombi. We have previously shown that fusion of anti-platelet and/or thrombolytic drugs to activated-platelet–targeting antibodies can provide an effective and safe alternative, delivering a localized high concentration at the site of the thrombus, thereby providing therapy and at the same time allowing a low systemic concentration, and so preventing bleeding complications[17,18]. In this study, we extend our previously successful therapeutic targeting to a successful targeted molecular theranostic approach with a single bolus injection for concurrent diagnosis and therapy of thrombotic diseases.

To avoid the safety concerns of sonoporation, we conjugated both the activated targeted scFvs and the thrombolytic agents to the outside of the MBs. This dual conjugation allowed the TT-MBs to be directed and to bind to the blood clot, and for the scuPA on the surface to react with the thrombus, and for thrombolysis to occur. Although the use of sonoporation for sonothrombolysis might have the potential to enhance the degree of thrombolysis, our study has been designed to avoid the disadvantages associated with the bursting of microbubbles. Our approach allows us to have good visualization of the thrombi on real-time ultrasound imaging. In addition to making it possible to directly monitor the reduction in thrombus size, this approach also notably eliminates the potential hemorrhagic complication associated with sonothrombolysis as noted in several studies[16,27].

There are several clinical scenarios in which ultrasound imaging with targeted theranostic microbubbles could be useful. Of these, the most important is MI. A method with fast diagnosis of coronary thrombi, together with rapid and "safe" thrombolysis using the theranostic microbubbles, has enormous potential to change outcomes for patients with MI on a large scale. Furthermore, this theranostic technique could be used to determine the success or failure of the applied thrombolysis, allowing an early decision toward direct invasive coronary angiography with consequent angioplasty and stenting. With the general access to ultrasound machines, the described theranostic ultrasound microbubbles can potentially be administered quickly and easily in emergency departments, and even in ambulances and remote clinics. Further studies toward clinical implementation of such a strategy are highly warranted.

Limitations

In this proof of concept study, we have used biotin/streptavidin coupling to conjugate scFv and scuPA onto microbubbles. This conjugation method offers major advantages such as flexibility and rapid coupling. Although there have been concerns regarding the potential immunogenicity that may limit the use of this coupling approach in humans, biotinylated drugs and avidin-based reagents have been recently successfully introduced in the clinic[50,51]. Nevertheless, as a potential alternative, our group has been developing novel enzymatic bioconjugation techniques for coupling, such as the use of the *S. aureus* transpeptidase sortase A, which can be adapted for use with our theranostic ultrasound molecular imaging approach[14,19,20].

Our study was conducted in a mouse model, which may not reflect thrombogenesis in humans in all aspects. Therefore further studies using bigger

animals and ultrasound scanners, as well as transducers typically used in patients, would facilitate further advancing this novel theranostic approach to clinical application. For this reason, we investigated additional cross-reactivity of our targeting single-chain antibody. We could show selective binding of the $scFv_{anti\text{-}LIBS}$ to activated platelets of non-human primates (data not shown). Hence, the $scFv_{anti\text{-}LIBS}$ not only shows cross-reactivity in humans and mice but also in non-human primates, which will facilitate translation of the newly described molecular ultrasound theranostic approach into clinical application in patients.

Conclusions

Our study demonstrates the successful generation of targeted theranostic microbubbles which bind specifically to activated platelets both *in vitro* and *in vivo*, thereby facilitating ultrasound molecular imaging of thrombi, as well as clot-localized enrichment of fibrinolytic activity. Thrombus size can be directly visualized in real time, offering unprecedented early diagnosis and monitoring of success or failure of thrombolytic therapy. Notably, single-chain antibody–mediated targeting allows enrichment at the thrombus site and at the same time a low systemic concentration of fibrinolytic activity, promising high thrombolytic efficacy without bleeding complications. This proof of concept study justifies further, particularly clinical, development and testing of this theranostic thrombolytic agent/ imaging microbubble for ultrasound diagnosis and targeted therapy of thrombotic disease in patients.

Supplementary Material

Additional File 1:
Supplemental Methods, Supplemental Results, Supplemental Figures 1-3.
http://www.thno.org/v06p0726s1.pdf
Additional File 2:
Video 1. http://www.thno.org/v06p0726s2.avi
Additional File 3:
Video 2. http://www.thno.org/v06p0726s3.avi
Additional File 4:
Video 3. http://www.thno.org/v06p0726s4.avi
Additional File 5:
Video 4. http://www.thno.org/v06p0726s5.avi

Acknowledgements

We would like to thank K. Alt and J. Yao for advice and technical support.

Sources of funding

This work was funded by the National Health and Medical Research Council (NHMRC) project grant 1050018 (K.P.) and the National Heart Foundation (NHF) Grant-in-Aid G05M2134 (K.P.); an Australian Research Council Future Fellowship (K.P.), NHMRC Principal Research Fellowships (K.P.), NHF Career Development Fellowship (C.E.H) and a NHF Postdoctoral Fellowships (X.W. and YC.C.). Y.G was supported by a stipend from the Deutsche Herzstiftung. The study was supported in part by the Victorian Government's Operational Infrastructure Support Program.

Competing Interests

The authors have declared that no competing interest exists.

References

1. Weber C, Noels H. Atherosclerosis: current pathogenesis and therapeutic options. *Nat Med*. 2011;17:1410–1422.
2. Mackman N. Triggers, targets and treatments for thrombosis. *Nature*. 2008;451:914–918.
3. Rader DJ, Daugherty A. Translating molecular discoveries into new therapies for atherosclerosis. *Nature*. 2008;451:904–913.
4. Lindemann S, Krämer B, Seizer P, Gawaz M. Platelets, inflammation and atherosclerosis. *J Thromb Haemost JTH*. 2007;5 Suppl 1:203–211.
5. Lindner JR. Molecular imaging of thrombus: technology in evolution. *Circulation*. 2012;125:3057–3059.
6. Schwarz M, Meade G, Stoll P, Ylanne J, Bassler N, Chen YC, Hagemeyer CE, Ahrens I, Moran N, Kenny D, Fitzgerald D, Bode C, Peter K. Conformation-specific blockade of the integrin GPIIb/IIIa: a novel antiplatelet strategy that selectively targets activated platelets. *Circ Res*. 2006;99:25–33.
7. Armstrong PC, Peter K. GPIIb/IIIa inhibitors: from bench to bedside and back to bench again. *Thromb Haemost*. 2012;107:808–814.
8. Stoll P, Bassler N, Hagemeyer CE, Eisenhardt SU, Chen YC, Schmidt R, Schwarz M, Ahrens I, Katagiri Y, Pannen B, Bode C, Peter K. Targeting ligand-induced binding sites on GPIIb/IIIa via single-chain antibody allows effective anticoagulation without bleeding time prolongation. *Arterioscler Thromb Vasc Biol*. 2007;27:1206–1212.
9. von Elverfeldt D, Maier A, Duerschmied D, Braig M, Witsch T, Wang X, Mauler M, Neudorfer I, Menza M, Idzko M, Zirlik A, Heidt T, Bronsert P, Bode C, Peter K, von Zur Muhlen C. Dual-contrast molecular imaging allows noninvasive characterization of myocardial ischemia/reperfusion injury after coronary vessel occlusion in mice by magnetic resonance imaging. *Circulation*. 2014;130:676–687.
10. von zur Muhlen C, von Elverfeldt D, Moeller JA, Choudhury RP, Paul D, Hagemeyer CE, Olschewski M, Becker A, Neudorfer I, Bassler N, Schwarz M, Bode C, Peter K. Magnetic resonance imaging contrast agent targeted toward activated platelets allows in vivo detection of thrombosis and monitoring of thrombolysis. *Circulation*. 2008;118:258–267.
11. von zur Muhlen C, Peter K, Ali ZA, Schneider JE, McAteer MA, Neubauer S, Channon KM, Bode C, Choudhury RP. Visualization of activated platelets by targeted magnetic resonance imaging utilizing conformation-specific antibodies against glycoprotein IIb/IIIa. *J Vasc Res*. 2009;46:6–14.
12. von Zur Muhlen C, Sibson NR, Peter K, Campbell SJ, Wilainam P, Grau GE, Bode C, Choudhury RP, Anthony DC. A contrast agent recognizing activated platelets reveals murine cerebral malaria pathology undetectable by conventional MRI. *J Clin Invest*. 2008;118:1198–1207.
13. Alt K, Paterson BM, Ardipradja K, Schieber C, Buncic G, Lim B, Poniger SS, Jakoby B, Wang X, O'Keefe GJ, Tochon-Danguy HJ, Scott AM, Ackermann U, Peter K, Donnelly PS, Hagemeyer CE. Single-chain antibody conjugated to a cage amine chelator and labeled with positron-emitting copper-64 for diagnostic imaging of activated platelets. *Mol Pharm*. 2014;11:2855–2863.
14. Wang X, Hagemeyer CE, Hohmann JD, Leitner E, Armstrong PC, Jia F, Olschewski M, Needles A, Peter K, Ahrens I. Novel Single-Chain Antibody-Targeted Microbubbles for Molecular Ultrasound Imaging of Thrombosis: Validation of a Unique Noninvasive Method for Rapid and Sensitive Detection of Thrombi and Monitoring of Success or Failure of Thrombolysis in Mice. *Circulation*. 2012;125:3117–3126.
15. Collen D, Lijnen HR. The tissue-type plasminogen activator story. *Arterioscler Thromb Vasc Biol*. 2009;29:1151–1155.
16. Donnan GA, Davis SM, Parsons MW, Ma H, Dewey HM, Howells DW. How to make better use of thrombolytic therapy in acute ischemic stroke. *Nat Rev Neurol*. 2011;7:400–409.
17. Hohmann JD, Wang X, Krajewski S, Selan C, Haller CA, Straub A, Chaikof EL, Nandurkar HH, Hagemeyer CE, Peter K. Delayed targeting of CD39 to activated platelet GPIIb/IIIa via a single-chain antibody: breaking the link between antithrombotic potency and bleeding? *Blood*. 2013;121:3067–3075.
18. Wang X, Palasubramaniam J, Gkanatsas Y, Hohmann JD, Westein E, Kanojia R, Alt K, Huang D, Jia F, Ahrens I, Medcalf RL, Peter K, Hagemeyer CE. Towards effective and safe thrombolysis and thromboprophylaxis: preclinical testing of a novel antibody-targeted recombinant plasminogen activator directed against activated platelets. *Circ Res*. 2014;114:1083–1093.

19. Ta HT, Prabhu S, Leitner E, Jia F, von Elverfeldt D, Jackson KE, Heidt T, Nair AKN, Pearce H, von Zur Muhlen C, Wang X, Peter K, Hagemeyer CE. Enzymatic single-chain antibody tagging: a universal approach to targeted molecular imaging and cell homing in cardiovascular disease. *Circ Res*. 2011;109:365–373.
20. Hagemeyer CE, Alt K, Johnston APR, Such GK, Ta HT, Leung MKM, Prabhu S, Wang X, Caruso F, Peter K. Particle generation, functionalization and sortase A–mediated modification with targeting of single-chain antibodies for diagnostic and therapeutic use. *Nat Protoc*. 2014;10:90–105.
21. Hagemeyer CE, von Zur Muhlen C, von Elverfeldt D, Peter K. Single-chain antibodies as diagnostic tools and therapeutic agents. *Thromb Haemost*. 2009;101:1012–1019.
22. Eisenhardt SU, Schwarz M, Bassler N, Peter K. Subtractive single-chain antibody (scFv) phage-display: tailoring phage-display for high specificity against function-specific conformations of cell membrane molecules. *Nat Protoc*. 2007;2:3063–3073.
23. Leuschner F, Nahrendorf M. Molecular imaging of coronary atherosclerosis and myocardial infarction: Considerations for the bench and perspectives for the clinic. *Circ Res*. 2011;108:593–606.
24. Pysz MA, Foygel K, Rosenberg J, Gambhir SS, Schneider M, Willmann JK. Antiangiogenic Cancer Therapy: Monitoring with Molecular US and a Clinically Translatable Contrast Agent (BR55)1. *Radiology*. 2010;256:519–527.
25. Metzger K, Vogel S, Chatterjee M, Borst O, Seizer P, Schönberger T, Geisler T, Lang F, Langer H, Rheinlaender J, Schäffer TE, Gawaz M. High-frequency ultrasound-guided disruption of glycoprotein VI-targeted microbubbles targets atheroprogressison in mice. *Biomaterials*. 2015;36:80–89.
26. Liu Y, Davidson BP, Yue Q, Belcik T, Xie A, Inaba Y, McCarty OJT, Tormoen GW, Zhao Y, Ruggeri ZM, Kaufmann BA, Lindner JR. Molecular imaging of inflammation and platelet adhesion in advanced atherosclerosis effects of antioxidant therapy with NADPH oxidase inhibition. *Circ Cardiovasc Imaging*. 2013;6:74–82.
27. McCarty OJT, Conley RB, Shentu W, Tormoen GW, Zha D, Xie A, Qi Y, Zhao Y, Carr C, Belcik T, Keene DR, de Groot PG, Lindner JR. Molecular imaging of activated von Willebrand factor to detect high-risk atherosclerotic phenotype. *JACC Cardiovasc Imaging*. 2010;3:947–955.
28. Reperfusion therapy for acute myocardial infarction with fibrinolytic therapy or combination reduced fibrinolytic therapy and platelet glycoprotein IIb/IIIa inhibition: the GUSTO V randomised trial. *The Lancet*. 2001;357:1905–1914.
29. de Saint Victor M, Crake C, Coussios C-C, Stride E. Properties, characteristics and applications of microbubbles for sonothrombolysis. *Expert Opin Drug Deliv*. 2014;11:187–209.
30. Tachibana K, Tachibana S. Albumin microbubble echo-contrast material as an enhancer for ultrasound accelerated thrombolysis. *Circulation*. 1995;92:1148–1150.
31. Culp WC, Flores R, Brown AT, Lowery JD, Roberson PK, Hennings LJ, Woods SD, Hatton JH, Culp BC, Skinner RD, Borrelli MJ. Successful microbubble sonothrombolysis without tissue-type plasminogen activator in a rabbit model of acute ischemic stroke. *Stroke J Cereb Circ*. 2011;42:2280–2285.
32. Porter TR, LeVeen RF, Fox R, Kricsfeld A, Xie F. Thrombolytic enhancement with perfluorocarbon-exposed sonicated dextrose albumin microbubbles. *Am Heart J*. 1996;132:964–968.
33. Xie F, Slikkerveer J, Gao S, Lof J, Kamp O, Unger E, Radio S, Matsunaga T, Porter TR. Coronary and microvascular thrombolysis with guided diagnostic ultrasound and microbubbles in acute ST segment elevation myocardial infarction. *J Am Soc Echocardiogr*. 2011;24:1400–1408.
34. Xie F, Lof J, Matsunaga T, Zutshi R, Porter TR. Diagnostic ultrasound combined with glycoprotein IIb/IIIa-targeted microbubbles improves microvascular recovery after acute coronary thrombotic occlusions. *Circulation*. 2009;119:1378–1385.
35. Kutty S, Xie F, Gao S, Drvol LK, Lof J, Fletcher SE, Radio SJ, Danford DA, Hammel JM, Porter TR. Sonothrombolysis of intra-catheter aged venous thrombi using microbubble enhancement and guided three-dimensional ultrasound pulses. *J Am Soc Echocardiogr*. 2010;23:1001–1006.
36. Alonso A, Dempfle C-E, Martina A Della, Stroick M, Fatar M, Zohsel K, Allémann E, Hennerici MG, Meairs S. In vivo clot lysis of human thrombus with intravenous abciximab immunobubbles and ultrasound. *Thromb Res*. 2009;124:70–74.
37. Greineder CF, Howard MD, Carnemolla R, Cines DB, Muzykantov VR. Advanced drug delivery systems for antithrombotic agents. *Blood*. 2013;122:1565–1575.
38. Zaitsev S, Spitzer D, Murciano J-C, Ding B-S, Tliba S, Kowalska MA, Marcos-Contreras OA, Kuo A, Stepanova V, Atkinson JP, Poncz M, Cines DB, Muzykantov VR. Sustained thromboprophylaxis mediated by an RBC-targeted pro-urokinase zymogen activated at the site of clot formation. *Blood*. 2010;115:5241–5248.
39. Ding B-S, Hong N, Murciano J-C, Ganguly K, Gottstein C, Christofidou-Solomidou M, Albelda SM, Fisher AB, Cines DB, Muzykantov VR. Prophylactic thrombolysis by thrombin-activated latent prourokinase targeted to PECAM-1 in the pulmonary vasculature. *Blood*. 2008;111:1999–2006.
40. Peter K, Graeber J, Kipriyanov S, Zewe-Welschof M, Runge MS, Kübler W, Little M, Bode C. Construction and functional evaluation of a single-chain antibody fusion protein with fibrin targeting and thrombin inhibition after activation by factor Xa. *Circulation*. 2000;101:1158–1164.
41. Unger E, Porter T, Lindner J, Grayburn P. Cardiovascular drug delivery with ultrasound and microbubbles. *Adv Drug Deliv Rev*. 2014;72:110–126.
42. Nishioka T, Luo H, Fishbein MC, Cercek B, Forrester JS, Kim CJ, Berglund H, Siegel RJ. Dissolution of thrombotic arterial occlusion by high intensity, low frequency ultrasound and dodecafluoropentane emulsion: an in vitro and in vivo study. *J Am Coll Cardiol*. 1997;30:561–568.
43. Birnbaum Y, Luo H, Nagai T, Fishbein MC, Peterson TM, Li S, Kricsfeld D, Porter TR, Siegel RJ. Noninvasive in vivo clot dissolution without a thrombolytic drug: recanalization of thrombosed iliofemoral arteries by transcutaneous ultrasound combined with intravenous infusion of microbubbles. *Circulation*. 1998;97:130–134.
44. Alexandrov AV, Molina CA, Grotta JC, Garami Z, Ford SR, Alvarez-Sabin J, Montaner J, Saqqur M, Demchuk AM, Moyé LA, Hill MD, Wojner AW, CLOTBUST Investigators. Ultrasound-enhanced systemic thrombolysis for acute ischemic stroke. *N Engl J Med*. 2004;351:2170–2178.
45. Molina CA, Barreto AD, Tsivgoulis G, Sierzenski P, Malkoff MD, Rubiera M, Gonzales N, Mikulik R, Pate G, Ostrem J, Singleton W, Manvelian G, Unger EC, Grotta JC, Schellinger PD, Alexandrov AV. Transcranial ultrasound in clinical sonothrombolysis (TUCSON) trial. *Ann Neurol*. 2009;66:28–38.
46. Hua X, Zhou L, Liu P, He Y, Tan K, Chen Q, Gao Y, Gao Y. In vivo thrombolysis with targeted microbubbles loading tissue plasminogen activator in a rabbit femoral artery thrombus model. *J Thromb Thrombolysis*. 2014;38:57–64.
47. Hagisawa K, Nishioka T, Suzuki R, Maruyama K, Takase B, Ishihara M, Kurita A, Yoshimoto N, Nishida Y, Iida K, Luo H, Siegel RJ. Thrombus-targeted perfluorocarbon-containing liposomal bubbles for enhancement of ultrasonic thrombolysis: in vitro and in vivo study. *J Thromb Haemost*. 2013;11:1565–1573.
48. Schwarz M, Nordt T, Bode C, Peter K. The GP IIb/IIIa inhibitor abciximab (c7E3) inhibits the binding of various ligands to the leukocyte integrin Mac-1 (CD11b/CD18, alphaMbeta2). *Thromb Res*. 2002;107:121–128.
49. Peter K, Kohler B, Straub A, Ruef J, Moser M, Nordt T, Olschewski M, Ohman ME, Kübler W, Bode C. Flow cytometric monitoring of glycoprotein IIb/IIIa blockade and platelet function in patients with acute myocardial infarction receiving reteplase, abciximab, and ticlopidine: continuous platelet inhibition by the combination of abciximab and ticlopidine. *Circulation*. 2000;102:1490–1496.
50. Petronzelli F, Pelliccia A, Anastasi AM, Lindstedt R, Manganello S, Ferrari LE, Albertoni C, Leoni B, Rosi A, D'Alessio V, Deiana K, Paganelli G, De Santis R. Therapeutic use of avidin is not hampered by antiavidin antibodies in humans. *Cancer Biother Radiopharm*. 2010;25:563–570.
51. Equinox Investigators. Efficacy and safety of once weekly subcutaneous idrabiotaparinux in the treatment of patients with symptomatic deep venous thrombosis. *J Thromb Haemost JTH*. 2011;9:92–99.

Authors' Biography

Prof Karlheinz Peter MD, PhD, works as senior interventional cardiologist at the Alfred Hospital and as Associate Director and Head of the Atherothrombosis and Vascular Biology Program at Baker IDI Heart and Diabetes Institute, Melbourne, Australia. He is Professor of Medicine and Immunology at Monash University and is a NHMRC principal research fellow. He obtained his research and clinical training in at the Universities of Freiburg and Heidelberg in Germany and at Johns Hopkins Medical School and Scripps Research Institute in the US. His research is focused on the cellular mechanisms, prevention and novel therapeutic approaches in myocardial infarction, encompassing the role of platelets, coagulation and inflammation in atherosclerosis, as well as the mechanisms leading to the rupture of atherosclerotic plaques. Using recombinant antibody technologies he has developed novel biomarker and molecular imaging strategies using magnetic resonance imaging (MRI), positron emission tomography (PET)/CT, ultrasound and fluorescence imaging as well as novel antithrombotic and fibrinolytic approaches that are not associated with increased bleeding risks. Prof Peter has received numerous awards throughout his career, including the Ludwig Heilmeyer Prize of the University of Freiburg, the Oskar Lapp Prize of the German Cardiac Society, the Ross Hohnen award of the Australian Heart Foundation, and the RT Hall Prize of the Cardiac Society of Australia and New Zealand.

Dr Xiaowei Wang is a postdoctoral fellow at the Baker IDI Heart and Diabetes Institute, Melbourne, Australia. She was trained as a sonographer for echocardiography prior to her research career therefore Dr Wang's research has a strong focus on translational cardiovascular research in diagnostics, therapeutics and theranostics. Dr Wang was awarded

a Postdoctoral Fellowship and the Paul Korner Innovation Award by the National Heart Foundation. She has received numerous young investigator awards and travel grants for international conferences. Dr Wang is also one of the founding board members of the Australia Society of Molecular Imaging.